

Highly efficient conversion of methane using microsecond and nanosecond pulsed spark discharges

Yuan Gao^{a, b, *}, Shuai Zhang^{a, b, *}, Hao Sun^{a, c}, Ruixue Wang^{a, b}, Xin Tu^d, Tao Shao^{a, b, c, **}

^a Institute of Electrical Engineering, Chinese Academy of Sciences, Beijing 100190, China

^b Key Laboratory of Power Electronics and Electric Drive, Chinese Academy of Sciences, Beijing 100190, China

^c University of Chinese Academy of Sciences, Beijing 100049, China

^d Department of Electrical Engineering and Electronics, University of Liverpool, Liverpool, L69 3GJ, United Kingdom

* Co-first authors.

** Corresponding author. Tel: +86 10 82547114, Email address: st@mail.iee.ac.cn

ABSTRACT: Plasma-assisted methane (CH₄) activation is a promising way for a hydrogen (H₂) production. In this paper, we describe our studies of microsecond and nanosecond pulsed spark discharge plasmas use in a CH₄ pyrolysis for a H₂ production. The dependence of CH₄ conversion and gas discharge product composition on discharge power, discharge gap length and gas flow rate are studied. The electrical and optical characteristics of the discharges are also studied to reveal discharge plasma parameters and chemical reactions leading to CH₄ pyrolysis. Experimental results show that H₂ and acetylene (C₂H₂) are the major gas discharge products accompanied by trace gas discharge products, such as ethane (C₂H₆), ethylene (C₂H₄) and carbon. **The highest CH₄ conversion and H₂ yield, 91.2% and 38.4%, respectively, are achieved with an energy conversion efficiency of 44.3% using the microsecond pulsed spark discharge at a gap length 6 mm and a gas flow rate 50 mL/min.** The carbon balance under the studied operating parameters varies from 66.7% to 92.8%. The morphology of carbon deposition is presented by two crystal forms identified by SEM and Raman spectral analyses. Finally, comparatively low electron temperature and high vibrational molecular temperature are observed in our experiments, which suggests that V-V transition for CH₄ excitation process and V-T transition for CH₄ heating process play important roles in CH₄ pyrolysis sustained by the pulsed spark discharge.

Keywords: Microsecond pulsed spark discharge; nanosecond pulsed spark discharge; needle-to-plate discharge reactor; CH₄ pyrolysis; H₂ production.

1. Introduction

The rapid exhaustion of fossil fuel reserves (petroleum and coal) and the increased energy requirements cause serious energy and environmental problems associated with the greenhouse CO₂ emissions. The development of new and emerging clean energy technologies [1-3], such as use of a natural gas whose annual production grows up to 4.5×10^{12} m³ worldwide [4], is essential and may play an important role in the future. Clean and efficient utilization of natural gas resources require a process wherein the CH₄ is selectively converted into a range of value-added sub-products, such as H₂, C₂H₄, C₂H₂ and methanol (CH₃OH) [5-7]. However, CH₄ is characterized by high C–H bond strength (435 kJ/mol), negligible electron affinity, high ionization energy, and weak polarizability [8]. In the last century, various chemical technologies had been developed for converting CH₄ into H₂ and other value-added chemicals [8-10]. In the beginning of this century, Guo et al. [11] developed a novel catalyst with single iron molecules embedded in a silica matrix at 1363 K for direct, non-oxidative conversion of CH₄ with maximum CH₄ conversion 48.4% and total hydrocarbon selectivity 99%. However, the high temperature of the process and high costs of manufacturing the highly active and stable catalyst remain the main challenges for that type of CH₄ conversion in a commercial scale [12].

Low-temperature plasma (LTP) provides a promising alternative route to tackle the challenges in CH₄ activation and conversion [13-15]. LTP systems can directly excite, dissociate and ionize CH₄ molecules [16-19] to create a range of reactive species, including vibrationally and electronically excited species and radicals [20-23], at a comparatively low-temperatures. In the past decades, various LTP systems, such as spark discharge [24-25], dielectric barrier discharge (DBD) [26], gliding arc discharge (GAD) [27-29], radio frequency (RF) discharge [30-31], microwave (MW) discharge [32-33], and corona discharge [22, 34] had been used for the conversion of CH₄. Thanyachotpaiboon et al. [22] investigated the direct conversion of CH₄ to higher hydrocarbons using an AC LTP system and obtained

a highest conversion efficiency 25% at an applied voltage 11 kV. Kado et al. [24] evaluated the direct conversion of CH₄ by comparing pulsed DC DBD, corona discharge and spark discharge and found that the energy efficiency of plasma process using the spark discharge, 32.3%, was three times as much as that if using DBD and corona discharge. Li et al. [25] developed a stable kilohertz spark discharge system for high energy-efficient conversion of CH₄ to H₂ and C₂H₂ and obtained the energy costs 6.6 – 10.7 eV per CH₄ molecule converted, 4.4 – 6.7 eV per H₂ molecule, and 16.9 – 27.6 eV per C₂H₂ molecule produced. Dae Hoon et al. [29] designed a rotating GAD system to evaluate the influence of arc length on C₂ selectivity and suggested that the arc length plays an important role in the controlling of ambient temperature and chemical reaction. Higher-energy LTP excited by RF and MW power sources were employed to CH₄ conversion for a better conversion performance, especially for the pyrolysis of CH₄ hydrate [30]. Jasiński et al. [32] converted CH₄ with MW power of few kilowatts at a gas flow rate of thousands L/h and obtained H₂ production rate and energy efficiency of H₂ production of about 600 NL [H₂]/h and 200 NL [H₂]/kWh, respectively. Putra et al. [31] and Rahim et al. [33] investigated CH₄ reforming using RF and MW plasmas and showed that H₂ content of 55% can be obtained in RF plasma at 150 W and that microwave plasma optimizes pyrolysis of CH₄ at a fast-emitted rate.

Series of experiments mentioned above are mostly conducted with DC, AC, RF or MW power sources, when the injected power is used for heating CH₄ molecules in the discharge area, which results in considerable energy losses. In recent years, however, pulsed discharge plasma has become an important subject of academic research and applications [36-39]. Especially, the ultra-fast repetitive pulsed discharges have been rapidly developed and used in many applications, such as H₂ generation [40-42], surface modification [43], heavy oil catalytic-cracking [44] and VOC degradation [45]. The repetitive pulses initiate discontinuous discharge that prevents remarkable heat losses between pulses and improves, by such a way, the discharge stability and the energy efficiency without overheating effect.

Nishida et al. [46] investigated the influence of a pulse power source on efficient H₂ production from CH₄, and showed that the microsecond pulses can effectively enhance the conversion efficiency. Khalifeh et al. [47-48] studied the pyrolysis of CH₄ using a nanosecond pulsed plasma in a cylindrical DBD reactor and found that the maximum CH₄ conversion 87% and H₂ yield 80% can be achieved at the average input power 268 W. Scapinello et al. [49] employed a nanosecond pulsed plasma for CH₄ and CO₂ reforming and achieved an energy efficiency up to 40%. Roussio et al. [50] developed a nanosecond pulsed discharge system for a low-temperature conversion processes of n-heptane and found that argon dilution induced by higher argon concentration enhanced the oxidation and pyrolysis of n-heptane by increasing the electron energy and electron density.

Thus, a high efficient and energy saving direct conversion of CH₄ to value-added chemicals is still considered to be a challenge. Although the thermal processes have demonstrated excellent conversion performances at high temperatures and high pressures, long cycle times, harsh conditions, and complicated reprocessing of these technologies can't be neglected. The LTP technology is also considered as a potential direct CH₄ conversion method because of its easy operation, efficient reaction process and mild condition. It should be noted that the conversion and energy efficiency of cold plasmas (such as corona and DBD) are not as high as it is with warm plasmas (i.e. gliding arc, spark, MW, and RF) because of their low reaction temperature, stability, controllability, and other factors. However, the severe overheating effect in warm plasmas can result in coking processes, which may attenuate and terminate the reaction.

The pulsed plasma can be used to obtain excellent conversion performances and mitigate the coking problems. The stability and controllability of a discharge also may be enhanced larger duty cycle of a pulsed plasma. Moreover, the higher average electron energy induced by short-pulsed plasmas is more favorable to excite and dissociate CH₄ molecules and further improve energy efficiency.

In our previous work, we verified the advantage of repetitively pulsed discharge

plasma produced by microsecond and nanosecond duration pulse power sources for flow control and material modification [51-54]. It was also showed that the electro-thermal coupling effect played a dominated role in plasma chemical reactions. The pulse power sources are more favorable in controlling electro-thermal coupling effect comparing to the traditional DC, AC, RF, and MW power sources.

The core issue of CH₄ non-oxidation is to find an optimum condition to investigate the balanced relation between the conversion degree of reactant, energy efficiency and coking. The average electron temperature in electric-field and the gas temperature can be efficiently improved using pulse power sources. The coking process is also well suppressed when a considerable energy efficiency is achieved.

In this paper, we describe the experimental results of CH₄ non-oxidative conversion for H₂ production in a needle-to-plate discharge reactor using nanosecond and microsecond pulse power sources. The voltage-current characteristics and optical emission spectra of the plasmas, as well as CH₄ conversion and gas product distributions are evaluated using different pulse power sources, gap lengths and gas flow rates. The power consumption, plasma parameters, carbon and hydrogen balances and energy efficiency are estimated and the possible reaction approaches of CH₄ pyrolysis are explored.

2. Experimental setups and methods

2.1. Experiment

Fig. 1 shows the experimental setup consisting of a pulse power source, a needle-plate discharge reactor, an electrical measurement system, a gas supply with a flow control system, an optical emission spectrometer and a gas chromatograph. The microsecond (peak voltage 0–40 kV, rising time 500 ns and FWHM 300 ns) and nanosecond (peak voltage 0–30 kV, rising time 350 ns and FWHM 150 ns) pulse power sources are triggered with a repetition frequency varied from 1 to 5 kHz.

In the needle-to-plate discharge reactor, two PTFE connectors and O rings are used to fix and seal a quartz tube with an outer diameter 60 mm and wall thickness 4

mm. A stainless-steel plate (diameter 50 mm) and a rod (length 120 mm, diameter 4 mm) with a needle-head (radius of curvature 0.5 mm) are placed inside the quartz tube and used as ground and high voltage electrodes, respectively. The gap length between the needle and the plate electrode may be varied from 0 to 10 mm. The gap lengths of the nanosecond pulsed spark discharge are 4 mm, 6 mm, 8 mm and 10 mm, while those of the microsecond pulsed spark discharge are 2 mm, 4 mm and 6 mm. The applied voltage and the discharge current are measured by a high voltage Tektronix probe P6015A and a current Pearson probe 6595, respectively, and recorded by a Tektronix oscilloscope DPO 2024. Flow of CH₄ (99.999%) at various gas flow rates (50, 100, 150 and 200 mL/min) is controlled using a mass flow controller D07-19, SEVENSTAR. The discharge gas products are detected by a gas chromatograph GC-9900, HSPX with a flame ionization detector (FID), and a thermal conductivity detector (TCD).

The emission light from the reactor is directly detected using an optical fiber placed about 10 mm away from the discharge reactor. An optical emission spectrometer AvaSpec-3648-6 is used to record the emission spectra of the plasmas within the wavelength range from 200 to 900 nm with a resolution 0.06 nm. The morphology and structure of carbon deposition are determined using a scanning electron microscope Merlin Compact, ZEISS and a high spectral resolution analytical Raman microscope LabRAM HR Evolution, HORIBA.

2.2. Data analysis

The experimental procedure is performed as follows. The reactor is fed by the CH₄ flow for 5 minutes. Then, the high voltage is applied to the needle electrode for 10 minutes, during which time an equilibrium is reached, and then the gas discharge products are measured. Finally, the high voltage is turned off and the discharge reactor is cleaned by the CH₄ flow for 5 minutes before the next pyrolysis process starts again.

Experimental results for plasma-assisted CH₄ pyrolysis are characterized by CH₄ conversion, H₂ yield and selectivity, hydrocarbons yields and selectivities, and the

resulted carbon and hydrogen balances.

The CH₄ conversion X_{CH_4} , is calculated as follows:

$$X_{CH_4} (\%) = \frac{(F_{CH_4}^{in} - F^{out} \times C_{CH_4}^{out})}{F_{CH_4}^{in}} \times 100, \quad (1)$$

where $F_{CH_4}^{in}$ (mL/min) is CH₄ gas flow rate at the inlet of the reactor, F^{out} (mL/min) is total output gas flow rate at the outlet of the reactor, and $C_{CH_4}^{out}$ is the molar fraction of CH₄ in the output gas flow.

The selectivities and yields of H₂ (S_{H_2}) and hydrocarbons ($S_{C_xH_y}$) are calculated as follows:

$$\text{Yield}_{H_2} (\%) = \frac{F^{out} \times C_{H_2}^{out}}{2 \times F^{out} \times X_{CH_4}} \times 100, \quad (2)$$

$$\text{Yield}_{C_xH_y} (\%) = \frac{x \times F^{out} \times C_{C_xH_y}^{out}}{F_{CH_4}^{in} \times X_{CH_4}} \times 100, \quad (3)$$

$$\text{Selectivity}_{H_2} (\%) = \frac{F^{out} \times C_{H_2}^{out}}{2 \times F_{CH_4}^{in} \times X_{CH_4}} \times 100, \quad (4)$$

$$\text{Selectivity}_{C_xH_y} (\%) = \frac{x \times F^{out} \times C_{C_xH_y}^{out}}{F_{CH_4}^{in} \times X_{CH_4}} \times 100. \quad (5)$$

The yield is defined above as the ratio of the target products to all raw reactants, while the selectivity is defined as the ratio of raw reactants for the target products to all consumed reactant.

Carbon and hydrogen balances are calculated as follows:

$$\text{Carbon balance}(\%) = \sum_{X=2,3} \frac{F^{out} \times (x \times C_{C_xH_y}^{out} + C_{CH_4}^{out})}{F_{CH_4}^{in}} \times 100, \quad (6)$$

$$\text{Hydrogen balance}(\%) = \sum_{Y=2,4,6,8} \frac{F^{out} \times (y \times C_{C_xH_y}^{out} + 4 \times C_{CH_4}^{out} + 2 \times C_{H_2}^{out})}{4 \times F_{CH_4}^{in}} \times 100, \quad (7)$$

where x and y are the numbers of carbon and hydrogen atoms of hydrocarbons, respectively.

Specific energy input (*SEI*) and energy conversion efficiency (*ECE*) are calculated as follows:

$$SEI(\text{kJ/L}) = \frac{60 \times P_{\text{input}}}{F_{\text{CH}_4}^{\text{in}}}, \quad (8)$$

$$ECE = \frac{\text{moles}Y_{\text{H}_2} \times \text{LHV}_{\text{H}_2} + \text{moles}Y_{\text{C}_x\text{H}_y} \times \text{LHV}_{\text{C}_x\text{H}_y}}{P + \text{moles} \text{CH}_4 \times \text{LHV}_{\text{CH}_4}} \times 100\%, \quad (9)$$

where P_{input} is the input power of a pulsed spark discharge, $\text{moles}Y_{\text{H}_2}$ and $\text{moles}Y_{\text{C}_x\text{H}_y}$ are the molar quantities of H_2 and C_xH_y for a unit-time (1 second), and LHV_{H_2} and $\text{LHV}_{\text{C}_x\text{H}_y}$ are the low heat values of H_2 and C_xH_y .

3. Results and discussions

3.1. Pulsed discharge characteristics

Fig. 2 shows the typical waveforms of applied voltage, plasma current and instantaneous power consumptions of the nanosecond (Fig. 2a) and microsecond (Fig. 2b) pulsed spark discharges. One can see there that amplitudes of applied voltage and plasma current of the nanosecond pulsed spark discharge are 12.9 kV and 37.2 A, respectively (Fig. 2a), with unipolar plasma current behavior, while amplitudes of applied voltage and plasma current of the microsecond pulsed spark discharge are 12.1 kV and 13.3 A, respectively (Fig. 2b).

3.2. CH_4 flow conversion

H_2 and C_2H_2 are usually identified as the major discharge gas products in the CH_4 conversion, while light hydrocarbons, such as C_2H_4 and C_2H_6 , are identified as trace products only. However, results of our measurements shows that all hydrocarbons, C_2H_2 , C_2H_4 and C_2H_6 , are the major discharge gas products as well. Since the saturate peak of CH_4 indicates that GC/FID method is not suitable for the measurement of high CH_4 concentration, the GC/TCD method is used to detect the CH_4 concentration.

The discharge gas products detection at each specific condition has been

performed 3 times to achieve a satisfactory accuracy with an experimental error less than 2%. This value of that experimental error is considered as introducing a little effect on the measurement results because of the high CH₄ conversion.

3.2.1 Effect of gap length

Fig. 3a shows dependences of the conversion of CH₄ and the yields of gas product on the discharge gap length in the nanosecond pulsed spark discharge operated with a constant repetition rate 1 kHz at 50 mL/min CH₄ flow rate. It is clearly seen that conversion of CH₄ and yields of discharge gas product proportionally increase with the increase of discharge gap length. The maximum CH₄ conversion 54.5% and H₂ yield 17.9% are obtained in the nanosecond pulsed spark discharge with a gap length 10 mm. This is an expected result because both applied voltage and discharge power increase with the increase of the gap length at a fixed pulse repetition rate and gas flow rate. For example, the CH₄ conversion increases by 12.8% when the gap length increases from 4 mm to 6 mm.

Fig. 3b shows dependences of the selectivities of discharge gas products on the gap length in the nanosecond pulsed spark discharge. One can see that the H₂ selectivity increases with the increase of the gap length and reaches its maximum of 32.9% at the gap length 10 mm. The highest C₂H₂ selectivity 43.5% is obtained at the gap length 4 mm. The selectivities of C₂H₄ and C₂H₆ is maintained at 1.8% and 1.2%, respectively, almost independently on the gap length.

Fig. 3c shows dependences of the carbon and hydrogen balances on the gap length in the nanosecond pulsed spark discharge. It is seen that the carbon and hydrogen balance reach their maxima of 83.2% and 75.9%, respectively, at the gap length 4 mm, and then decrease by 12.9% and 15.9%, respectively, when the gap length increases to 10 mm. It is assumed that the incomplete carbon and hydrogen balances are caused by deposition of carbon and hydrocarbons on the electrodes, which is not included into the mass balance calculations due to the existing limitations of our measurement equipment. Different liquids, such as hydrochloric acid, alcohol, acetone, n-heptane, and so on, have been used to dissolve and clean

carbon and hydrocarbon depositions. However, the depositions seem not to be dissolved completely.

Fig. 4a shows dependences of the conversion of CH_4 and the yields of gas product on the gap length in the microsecond pulsed spark discharge operated with a constant repetition rate 1 kHz at a gas flow rate 50 mL/min. The CH_4 conversion and the yields of discharge gas product ultimately reach their saturation values, while show similar to the nanosecond pulsed spark discharge dependence when the gap length increases. For example, the highest CH_4 conversion 91.2% and H_2 yield 38.4% are obtained in the microsecond pulsed spark discharge at the gap length 6 mm, which is almost double of that in the nanosecond pulsed spark discharge at the same gap length.

Fig. 4b shows the dependences of the selectivities of the gas products on the gap length in the microsecond pulsed spark discharge. While C_2H_2 selectivity fluctuates slightly around 60% and H_2 and C_2H_4 selectivities fluctuate around 39% and 2%, C_2H_6 selectivity reduces from 0.2% to 0.1% with the gap length increase from 2 mm to 6 mm, respectively.

Fig. 4c shows the dependences of the carbon and hydrogen balances on the gap length in the microsecond pulsed spark discharge. It can be seen that both carbon and hydrogen balances achieve their maxima of 72.4 % and 46.7%, respectively, at 2 mm gap length, and slightly decrease by 3.8% and 3.3%, respectively, at 6 mm gap length. It should be also noted that the carbon balance is higher than the hydrogen balance and less depend on the gap length in the microsecond pulsed spark discharges, if compared with the nanosecond pulsed spark discharges under the same experimental conditions. The reduced carbon balance in the microsecond pulsed spark discharge may be associated with a higher generation rate of carbon deposition, when compared with the nanosecond pulsed spark discharge.

It is also observed that severe coking problems in the microsecond pulsed spark discharges at the gap lengths of 8 mm and 10 mm lead to the rapid carbon depositing processes on the ground electrode with subsequent suppressions of the

discharges.

3.2.2 Effect of gas flow rate

Fig. 5a shows dependences of CH₄ conversion and gas product yields on the gas flow rate on in the nanosecond pulsed spark discharge with a repetition frequency 1 kHz and a gap length 6 mm. It can be clearly seen that the increase of the gas flow rate significantly decreases CH₄ conversion and yields of the discharge gas products because of the reduced CH₄ residence time within the plasma area. It can also be seen that increase of the gas flow rate from 50 to 200 mL/min decreases the CH₄ conversion and H₂ yield from 44.3% and 13.5% to 10.6% and 4.3%, respectively. The maximum CH₄ conversion 44.3% is obtained at a gas flow rate 50 mL/min. It is reasonable to assume that a higher gas flow rate decreases the residence time of reactants in the discharge, which reduces the possibilities of collisions between electrons and CH₄ molecules and its intermediates subsequently. As it is indicated in the Fig 5b, the selectivities of gas products varies when the gas flow rate changes from 50 to 200 mL/min. The increase of the gas flow rate at a constant input power increases selectivities of gas products but decreases their production. The highest H₂ and C₂H₂ selectivities reaches 40.5% and 42.2%, respectively, at the gas flow rate 200 mL/min at a gap length 6 mm. Fig. 5b also shows that selectivities of C₂H₆ and C₂H₄ are less influenced by the changing the gas flow rate and stabilizes around 2% and 1%, respectively.

Fig. 5c shows dependences of the carbon and hydrogen balances on the gas flow rate in the nanosecond pulsed spark discharge. It could be seen that the maximum carbon and hydrogen balances reach 92.8 % and 92.6%, respectively, at a gas flow rate 200 mL/min, and then decrease by 20.9% and 25.5%, respectively, when the gas flow rate decreases down to 50 mL/min.

Fig. 6a shows dependences of CH₄ conversion and gas product yields on the gas flow rate in the microsecond pulsed spark discharge at a gap length 6 mm and a constant repetition rate 1 kHz. It is clearly seen there that CH₄ conversion and gas product yields in the microsecond pulsed spark discharge also increase with a

decrease of gas flow rate in the nanosecond pulsed spark discharge. Specifically, the highest CH₄ conversion 91.2% and H₂ yield 38.4% are obtained in the microsecond pulsed spark discharge at a gas flow rate 50 mL/min, which is more than twice of that achieved using the nanosecond pulsed spark discharge.

Fig. 6b shows dependences of selectivities of discharge gas products on the gas flow rate in the microsecond pulsed spark discharge. C₂H₂ selectivity varies from 63.4% to 48.8% when the gas flow rate changes from 50 to 150 mL/min. The maximum C₂H₂ selectivity 67.9% is still obtained at the gas flow rate 200 mL/min, which is different from the nanosecond spark discharge. H₂ selectivity fluctuates a little around 38% and selectivities of C₂H₆ and C₂H₄ are maintained at 1% and 2%, respectively.

As shown in Fig. 6c, the carbon and hydrogen balances in the microsecond pulsed spark discharge achieve their maxima of 83.3% and 65.6%, respectively, at a gas flow rate 200 mL/min. Then slightly decrease with decrease of the gas flow rate to 68.5% and 43.4%, respectively, at 50 mL/min.

3.3 Morphology and structure of carbon deposition

The graphite, as it is reported by Peng et al. [55], is the most thermo-dynamically stable allotrope of carbon. Reaction temperature over 3300 K is required for graphitization process of an amorphous carbons. However, the traditional high-temperature processes in DC and AC arc plasmas [56] can only provide a partial graphitization, while most of amorphous carbons are remain non-graphitizable. The filamentary micro discharge channels in microsecond and nanosecond pulsed spark discharges are formed only to the end of the pulse duration time ($< 1\mu\text{s}$), so their heating effect is much weaker than that in DC and AC arc plasmas. According to the researches of Hooshmand et al. [57] and Song et al. [58], the fast-rising pulsed voltage prevents local overheating of micro discharges and suppress the carbon deposition. In our experiments, however, more favorable conditions might exist for generation of carbon nano-tubes and carbon nano-fibers. To prove this assumption, the morphology and structure of carbon depositions on the ground

electrode are studied with scanning electron microscope (SEM) and Raman spectrometer.

The carbon depositing area could be classified into three types as determined by SEM and Raman spectrometers (Fig. 7): (1) carbon particles in the darkest zone in the central part of the discharge area; (2) carbons and hydrocarbon mixtures in a lighter-colored zone which surrounds the central area; (3) the unidentified carbon formed in the soot formation zone outside the yellow-colored zone. Fig. 7a shows that lots of carbon filaments are generated on surface of area (1). In contrast to the area (1), the carbon depositions in the area (2) are found to be mainly consisted of the micro-scale carbon particles, which formed into an annular region on the surface of ground electrode (Fig. 7b). The reason for different carbon formations in these two areas is caused by different discharge properties in these two areas. The central part of the area (1) has higher generation rate of discharge channels, which creates more energetic electrons and ionization excitation of CH_4 molecules. Higher electron temperatures are obtained in the stronger electric field of spark discharge in the area (1), which makes the CH_4 dehydrogenating process more completed and the carbon depositions formed only into filaments and other nano-scale structures. The discharge channels in the area (2) are less likely generated because of the longer distance to a needle electrode. Less energy is injected to accelerate electrons in this area, and more CH_2 and CH species are activated and recombined into hydrocarbons by energetic electrons with lower energy states. The carbon depositions are also less likely to suffer secondary damages from the discharges, so the surface of these micro-scale particles are smoother than those in the area (1).

The Raman spectra of the carbon depositions in the nanosecond pulsed spark discharges are shown in the right side of Fig. 7 for the quality evaluation of carbon structures. The intense G-band ($\sim 1580 \text{ cm}^{-1}$) emission caused by the stretching vibration mode of a sp^2 -like carbon is clearly seen in the measured spectra. The peak at $\sim 1340 \text{ cm}^{-1}$ (D-band) belongs to the Raman mode of the amorphous carbon

or defects in the wall structure. The Raman spectra also shows a band at 2650 cm^{-1} called the G' band attributed to the overtone of the D band [59]. The intensity ratio of the bands, I_D/I_G , gives a measure of the degree of crystallinity of the graphite layers, since decrease of the I_D/I_G ratios corresponds to lower fractions of a sp^3 -like carbon and, hence, to less structural defects.

Fig. 7a shows that there are more of the sp^3 hybridized carbon atoms presented in the area (1), which indicates the higher generation rate of amorphous carbons. More sp^2 bonding carbons with amorphous graphite structure are observed in the Fig. 7b, as compared to the images shown in Fig. 7a. The obtained I_D/I_G ratio of 1.1 in the area (1) of the carbon sample suggests that the graphitization degree of the nano-scale carbons is relatively low.

3.4. Energy efficiency of the plasma process

The CH_4 conversion energy efficiency in our experiments with microsecond and nanosecond pulsed spark discharges is calculated and compared with that obtained in other different discharges [24, 28, 34, 60, 61] by extracting relevant data from the literature and re-calculating it into SEI and ECE numbers using Eqs. (8) - (9). Fig. 8 shows various experimental results of SEI with CH_4 conversion and ECE. Our experimental results of CH_4 conversion are plotted in Fig. 8a as a function of SEI in the microsecond pulsed spark discharge (blue scatter) and in the nanosecond pulsed spark discharge (red scatter), along with the published data. It is clear seen in Fig. 8a that the CH_4 conversion in all the discharges (including our pulsed spark discharges) are proportional to the SEI. A higher SEI yields more of high energetic electrons, which initiate more intensive collisions between electrons and CH_4 molecules and generate more reactive species leading to the higher CH_4 conversion. Also, it is evident that CH_4 conversion in the microsecond pulsed spark discharge (blue scatter) is higher than that in the corona discharge, DBD and spark discharge driven by AC power supply, as well as in nanosecond spark discharge (red scatter) and microwave discharge. However, it is slightly lower than that in the GAD at the same SEI.

The *ECE* is plotted in Fig. 8b as a function of *SEI* the same way as it is done in Fig. 8a. It can be seen there that the *ECE* in the microsecond pulsed spark discharge is higher than that in the most other discharge types (AC driven corona, DBD and spark, nanosecond spark discharges and MW discharge), but slightly lower than that in the GAD at the same *SEI*. Furthermore, it is clear that the maximum *ECE* in the microsecond and nanosecond pulsed spark discharges occurs at *SEI* of 12.1 kJ/L and 13.2 kJ/L, respectively, with corresponding gas flow rate 50 mL/min at gap lengths 2 and 4 mm. The input power is higher at gap lengths 2 mm (in the microsecond pulsed spark discharge) and 4 mm (in the nanosecond pulsed spark discharge), while CH₄ conversion and product selectivity are lower than that at other gap lengths. Therefore, *ECEs* are maximum, according to Eq. (9).

CH₄ conversion and *ECE* in the microsecond pulsed spark discharge are higher than that in the nanosecond pulsed spark discharge which can be attributed to the different electron impact probability in different experiments.

The differential cross section of the incident electron scattering with energy transfer $\Delta\varepsilon$ to the valence electron can be described as following [13], according to the Rutherford Formula Eq. (10):

$$d\sigma_i = \frac{1}{(4\pi\varepsilon_0)^2} \frac{\pi e^4}{\varepsilon(\Delta\varepsilon)^2} d(\Delta\varepsilon). \quad (10)$$

The transferred energy exceeds the ionization potential and the direct ionization will take place when $\Delta\varepsilon \geq 1$. Eq. (10) is integrated into the expression for the ionization cross section by direct electron impact, which is known as the Thomson formula Eq. (11):

$$\sigma_i = \frac{1}{(4\pi\varepsilon_0)^2} \frac{\pi e^4}{(\Delta\varepsilon)^2} \left(\frac{1}{I} - \frac{1}{\varepsilon} \right). \quad (11)$$

Electrons initiated by high instantaneous power in the pulsed spark discharge are accelerated to a higher energies, $\varepsilon \gg 1$, where the Thomson cross section reduces

as $\sigma_i \sim 1/\varepsilon$. The decrease of the Thomson cross section σ_i , which determines the direct electron impact probability, is caused by higher instantaneous power and shorter pulse width of the nanosecond pulsed discharge. More energetic electrons are activated in the nanosecond spark discharge, but most of them move straightly to the ground electrode without impacting heavy particles, which results in the lower energy consumption of the nanosecond spark discharge.

3.5. Chemical Reaction of the plasma process

Optical emission spectrometry is used to diagnose the distribution of particles in their excited states and both the electron and the gas temperatures. Fig. 9 shows the typical optical emission spectra between 350 nm and 700 nm of the microsecond and nanosecond pulsed discharges. The spectra are dominated by H-Balmer lines, vibrational-rotational bands of C₂ Swan ($A^3\Pi_g - X^3\Pi_u$) and C⁺ ($^2D - ^2F$) [spectral line](#) [62]. The C₂ Swan ($d^3\Pi_g - a^3\Pi_u$, $\Delta v = -1$) is used to estimate the vibrational temperature of the pulsed spark discharge. The ratio of C₂ Swan ($A^3\Pi_g - X^3\Pi_u$, 563 nm) to C⁺ ($^2D - ^2F$, 427 nm) [spectral line](#) in the nanosecond pulsed spark discharge is lower than that in the microsecond pulsed spark discharge. It is seen in Fig. 9a that the H-Balmer lines are the most intense spectral lines in the nanosecond pulsed spark discharge, [which indicates that the dissociation of CH₄ leads to the formation of H radicals](#) [63].

[The electron temperature is estimated by calculating the Electron Energy Distribution Function \(EEDF\) using Boltzmann equation \[64\] and taking into account electron induced vibrational excitation of CH₄, electron induced dissociation of CH₄, electron-induced ionization of CH₄ and elastic impact between electron and CH₄, as shown in Fig. 10. While the Boltzmann plot method is still used to calculate electron temperature \[65\], it has been shown that it is not applicable to use in our experiments, where the discharge plasma is far from the equilibrium.](#)

[The time-average applied voltage and the gap length are used to calculate the electric field intensity \(E\). The reduced electric field \(E/N\) is defined then as the](#)

ratio of E to N , where the corresponding density of gas molecules (N) is calculated using the ideal gas state equation and the estimated gas temperature. An integrated Boltzmann equation solver BOLSIG+ is used to estimate the electron temperature (T_e) and the electron momentum (μ_e). The electric current density j_e is calculated using the time-average discharge current I and width of spark discharge channel d . A digital camera Canon 500D is used to capture the width of spark discharge channel d . The electron density (N_e) is calculated finally using CH_4 collision cross sections [66-68] as follows, Eqs. (12) – (14) [69-70]:

$$v_d = \mu_e \cdot E \text{ (cm} \cdot \text{s}^{-1}\text{)}. \quad (12)$$

$$j_e = \frac{4 \cdot I}{\pi \cdot d^2} \text{ (A} \cdot \text{cm}^{-2}\text{)}. \quad (13)$$

$$N_e = \frac{j_e}{e \cdot v_d} \text{ (cm}^{-3}\text{)}. \quad (14)$$

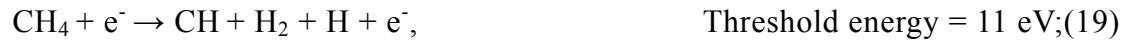
The calculated results and electrical properties of the pulsed power sources at different gap lengths are summarized in Table 1:

It is widely considered that the gas phases of a low-temperature plasma are characterized by a thermal non-equilibrium state and that the gas temperature is far less than the electron temperature. Generation of a low-temperature plasma is performed by series of steps, as described by Scapinello et al [71]. Initially, free electrons are accelerated to very high velocities by strong electrical field, which results in the electron temperature (T_e) of accelerated electrons usually ranged from 1 to 5 eV [71]. Then these energetic electrons collide with the gas molecules leading to excitation, dissociation, ionization and other plasma chemistry reactions of gas molecules in the energy-transfer processes [69]. The most important electron-impact reactions in the non-oxidation CH_4 conversion process include reactions listed below [72].

Vibrational excitations:



Dissociations:



Ionizations [73]:



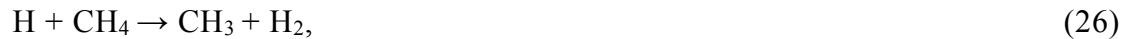
Only few energetic electrons participate in ionization because of the high energy requirements for the CH₄ ionization.

To understand the electron impact reactions in CH₄ non-oxidation process, Nozaki et al. developed a model describing fragmentation of CH₄ and polymerization process [74]. According to his research, the CH₄ dehydrogenation initiated by electrons is the main reaction, and CH₃ is the main radical with low reduced electric field (< 500 Td), although extremely CH₃ selectivity (60%) can even be obtained at 80 Td. The concentration of CH₃ radicals can be effectively increased at higher electron densities when the radical combination can also be enhanced by the high reactants (CH₃ radicals) concentration [75]:



However, the recombination of radicals results in plenty of heat and leads to a remarkable increase of the gas temperature. Dors et al. [76] developed a simplified model and pointed out that thermal effect should also be taken into consideration. The dehydrogenation reactions induced by H radicals play a dominated role in the

chemical kinetics of CH₄ conversion when the gas temperature is over 1000 K [75]:



The chemical reactions shown above explain the high selectivities of C₂H₂ and H₂. However, the electron impact dissociation should also be taken into consideration because of the high electron density in the pulsed discharges. The most remarkable vibrational – rotational spectral bands in the microsecond pulsed spark discharge is C₂ Swan (A³Π_g – X³Π_u) system (Fig. 9b), which results from formation of excited C₂ species due to the stronger thermal effect of vibrational excitation on CH₄ molecules. The overall thermal cracking reaction of CH₄ is achieved as follows [67]:



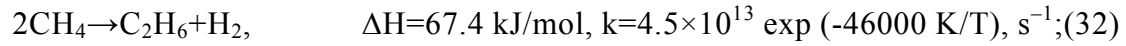
The longer rising time of the microsecond pulsed spark discharges, if comparing with the nanosecond pulsed spark discharge, reduces the number of high energetic electron collisions with lower energy states, so that the lower instantaneous power become not sufficient for CH₄ molecules dissociation through direct electron impact. The impact of electrons in the microsecond pulsed plasmas creates more ground state CH₄ molecules that transfers them to different vibrational levels (V13=0.36 eV, V24=0.16 eV) [70]. Finally, injected energy accumulation excites CH₄ molecules into high vibrational excited levels whose broken chemical bonds more easily converted into reactive radicals and other species.

As mentioned before, heavier hydrocarbons and soot are generated in the microsecond pulsed spark discharge, which indicates lower hydrogen balance of these microsecond pulsed spark discharge. According to the previous research [77], the thermal pyrolysis of CH₄ generally follows the mechanism suggested by Kassel,

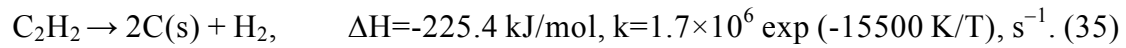
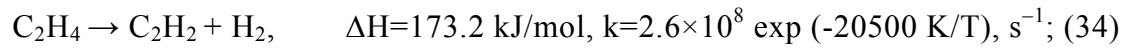
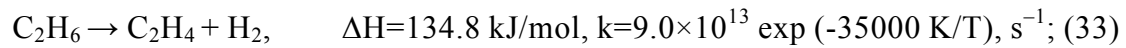
so the pyrolysis of CH₄ at high reacting temperatures forms CH₂ radicals, which is followed by the recombination of CH₂ with CH₄ into C₂H₆ [77]:



Overall reaction:



Further dehydrogenization results in a gradual conversion of C₂H₆ into C₂H₄ and then into C₂H₂, and finally conversion of C₂H₂ into soot [77]:



The electron energy increases at the reduced electrical field at the beginning of electron impact (Fig. 10). About 99% of the electrons with energies between 0.1 and 4 eV lost their energy into vibrational excitation of CH₄ molecules, due to their high vibrational excitation reaction cross section. The dissociation induced by excited electronic levels contributes much less, if comparing with the vibrational dissociation, due to its higher threshold and smaller cross section at low electron energies. The vibrational excitation cross section decreases dramatically at higher electron energies.

The average calculated electron energy of pulsed spark discharge is around 1.1 – 2.6 eV (Table. 1). The vibrational excitation cross section plays a dominant role in the energy loss and vibrational channels became the main dissociation mechanism of the molecules in the pulsed spark discharges. The vibrations dissipates their energy into translational or rotational degrees of freedom immediately after the main part of energy is transferred to vibrations by electrons. The CH₄ is thermally cracked into C₂H₆, C₂H₄, C₂H₂ and C(s) when the gas temperature rises to more than 1100 K.

Conclusions:

Different pulsed plasmas are generated in a needle-plate reactor to maintain the non-oxidation conversion of CH₄ at a desirable CH₄ conversion rate 91.2% and considerable energy efficiency 44.3%. Selective generation of the target product with improved stability, weaker overheats effect and higher energy efficiency by adjusting parameters of pulsed plasma is achieved.

H₂ production by direct conversion of CH₄ using microsecond and nanosecond pulsed spark discharges with a needle-plate electrode configuration is experimentally and parametrically investigated.

- (1) The maximum CH₄ conversion 91.2% and H₂ yield 38.4% with an *ECE* 44.3% are achieved using microsecond pulsed spark discharges, while the maximum carbon balance 92.8% and hydrogen balance 92.6% are obtained using nanosecond pulsed spark discharges.
- (2) CH₄ conversion and H₂ yield continue to increase with the gap length increase because of the increasing power consumption, and with the gas flow rate decrease because of the increased residence time in both nanosecond and microsecond pulsed spark discharges.
- (3) The carbon deposition is studied using SEM and Raman spectroscopy and classified into two different types. The high-value carbons are supposed to be formed in more sophisticated plasma systems.
- (4) Three chemical reaction are suggested to perform CH₄ pyrolysis at our experimental conditions. Higher effect of the thermal activation process is suggested to take place in the microsecond pulsed spark discharge because of the overriding selectivity of the C₂H₂.

The lab-scale and adjustable needle-plate reactor driven by repetitive high voltage pulse power sources is designed. The reactor is used for the direct conversion of greenhouse gas (CH₄) to renewable energy (H₂) and functional material (carbon material). The multi-needle to plate configuration of the reactor driven by nanosecond pulse power source can be also used for the H₂ generation or the carbon material production in the further research. The described experimental

procedure has a potential to improve selectivity of the plasma process by using a catalysis. It is believed to have huge potential in the C₂H₂ generation industries.

Acknowledgements:

Y. Gao and S. Zhang contributed equally to this work. This work is supported by National Natural Science Foundation of China (grant numbers 51637010, 51507169 and 51707186), The Royal Society – Newton Advanced Fellowship, UK (grant numbers NA140303) and Young Elite Scientists Sponsorship Program by CAST (grant numbers YESS20160025).

References:

- [1] Company B P. BP statistical review of world energy. London England British Petroleum Company 2015.
- [2] Reddy E L, Biju V M, Subrahmanyam C. Production of hydrogen and sulfur from hydrogen sulfide assisted by nonthermal plasma. *Applied Energy* 2012; 95: 87–92.
- [3] Hafizi A, Rahimpour M R, Hassanajili S. Hydrogen production via chemical looping steam methane reforming process: effect of cerium and calcium promoters on the performance of Fe₂O₃/Al₂O₃ oxygen carrier. *Applied Energy* 2016; 165: 685–94.
- [4] Zou C, Zhao Q, Zhang G, Xiong B. Energy revolution: from a fossil energy era to a new energy era. *Natural Gas Chemical Industry* 2016; 36(1): 1–10.
- [5] Song C F, Liu Q L, Ji N, Kansha Y, Tsutsumi A. Optimization of steam methane reforming coupled with pressure swing adsorption hydrogen production process by heat integration. *Applied Energy* 2015; 154: 392–401.
- [6] Zhao K, He F, Huang Z, Wei G, Zheng A, Li H. Perovskite-type oxides LaFe_xCo_xO₃ for chemical looping steam methane reforming to syngas and hydrogen coproduction. *Applied Energy* 2016; 168: 193–203.
- [7] Tseng P, Lee J, Friley P. A hydrogen economy: opportunities and challenges. *Energy* 2005; 30(14): 2703–2720.
- [8] Abbas H F, Daud W M A W. Hydrogen production by methane decomposition: a review. *International Journal of Hydrogen Energy* 2010; 35(3): 1160–1190.
- [9] Amin A M, Croiset E, Epling W. Review of methane catalytic cracking for hydrogen production. *International Journal of Hydrogen Energy* 2011; 36(4): 2904–2935.
- [10] Chaubey R, Sahu S, James O, Maity S. A review on development of industrial processes and emerging techniques for production of hydrogen from renewable and sustainable sources. *Renewable and Sustainable Energy Reviews* 2013; 23: 443–462.
- [11] Guo X, Fang G, Li G, Ma H, Fan H, Yu L, Ma C, Wu X, Deng D, Wei M, Tan D, Si R, Zhang S, Li J, Sun L, Tang Z, Pan X, B X. Direct, non-oxidative conversion of methane to ethylene, aromatics, and hydrogen. *Science* 2014; 344(2): 616–619.
- [12] Aba'nades A, Ruiz E, Ferruelo E M, Herná'ndez F, Cabanillas A, Martí'nez-Val J M, Rubio J A, Lo'pez C, Gavela R, Barrera G, Rubbia C, Salmieri D, Rodilla E, Gutie'rrez D. Experimental analysis of direct thermal methane cracking. *International Journal of Hydrogen*

Energy 2011; 36(20): 12877–12886.

- [13] Fridman A. Plasma chemistry. Cambridge (UK): Cambridge University Press; 2008, p. 16–17.
- [14] Petitpas G, Rollier J D, Darmon A, Gonzalez-Aguilar J, Metkemeijer R, Fulcheri L. A comparative study of non-thermal plasma assisted reforming technologies. *International Journal of Hydrogen Energy* 2007; 32(14): 2848–2867.
- [15] Rutberg P G, Kuznetsov V A, Popov V E, Sergey D P, Alexander V S, Dmitry I S, Alexander N B. Conversion of methane by $\text{CO}_2+\text{H}_2\text{O}+\text{CH}_4$ plasma. *Applied Energy* 2015; 148: 159–168.
- [16] Kogelschatz U. Filamentary, patterned, and diffuse barrier discharges. *IEEE Transaction on Plasma Science* 2002; 30(4): 1400–1408.
- [17] Xu S, Whitehead J C, Martin P A. CO_2 conversion in a non-thermal, barium titanate packed bed plasma reactor: The effect of dilution by Ar and N_2 . *Chemical Engineering Journal* 2017, 327: 764–773.
- [18] Chirokov A, Gutsol A, Fridman A. Atmospheric pressure plasma of dielectric barrier discharges. *Pure and applied chemistry* 2005; 77(2): 487–495.
- [19] Tendero C, Tixier C, Tristant P, Desmaison J, Leprince P. Atmospheric pressure plasmas: A review. *Spectrochimica Acta Part B: Atomic Spectroscopy* 2006; 61(1): 2–30.
- [20] Li X, Zhao H, Jia P, Bao W. A large gap uniform discharge excited by a direct-current voltage at atmospheric pressure. *Applied Physics Letters* 2013; 102(22): 223501.
- [21] Li X, Bao W, Chu J, Zhang P, Jia P. A uniform laminar air plasma plume with large volume excited by an alternating current voltage. *Plasma Sources Science and Technology* 2015; 24(6): 065020.
- [22] Thanyachotpaiboon K, Chavadej S, Caldwell T A, Lobban L L, Mallinson R G. Conversion of methane to higher hydrocarbons in AC non-equilibrium plasmas. *AIChE Journal* 1998; 44(10): 2252–2257.
- [23] Zhao G, John S, Zhang J, Wang L, Muknahallipatna S, Jerry C H, John F A, Morris D A, Ovid A P. Methane conversion in pulsed corona discharge reactors. *Chemical Engineering Journal* 2006; 125(2): 67–79.
- [24] Kado S, Sekine Y, Nozaki T, Okazaki K. Diagnosis of atmospheric pressure low temperature plasma and application to high efficient methane conversion. *Catalysis Today* 2004; 89(1): 47–55.
- [25] Li X, Lin C, Shi C, Xu Y, Wang Y, Zhu A. Stable kilohertz spark discharges for high-efficiency conversion of methane to hydrogen and acetylene. *Journal of Physics D: Applied Physics* 2008; 41: 175203.
- [26] Nozaki T, Okazaki K. Innovative Methane Conversion Technology Using Atmospheric Pressure Non-thermal Plasma. *Journal of the Japan Petroleum Institute* 2011; 54(3): 146–158.
- [27] Bidgoli A M, Ghorbanzadeh A, Lotfalipour R, Roustaei E, Zakavi M. Gliding spark plasma: Physical principles and performance in direct pyrolysis of methane. *Energy* 2017; 125: 705–715.
- [28] Indarto A, Choi J W, Lee H, Song H K. Effect of additive gases on methane conversion using gliding arc discharge. *Energy* 2006; 31(14): 2986–2995.
- [29] Lee D H, Kim K T, Min S C, et al. Plasma-controlled chemistry in plasma reforming of

- methane. *International Journal of Hydrogen Energy* 2010; 35(20): 10967–10976.
- [30] Bae J, Lee M, Park S, Jeong M G, Hong D Y, Kim Y D, Park Y K, Hwang Y K. Investigation of intermediates in non-oxidative coupling of methane by non-thermal RF plasma. *Catalysis Today* 2017; 294: 105–112.
- [31] Putra A E, Nomura S, Mukasa S, Toyota H. Hydrogen production by radio frequency plasma stimulation in methane hydrate at atmospheric pressure. *International Journal of Hydrogen Energy* 2012; 37(21): 16000–16005.
- [32] Jasiński M, Czylkowski D, Hrycak B, Dors M, Mizeraczyk J. Atmospheric pressure microwave plasma source for hydrogen production. *International Journal of Hydrogen Energy* 2013; 38(26): 11473–11483.
- [33] Rahim I, Nomura S, Mukasa S, Toyota H. Decomposition of methane hydrate for hydrogen production using microwave and radio frequency in-liquid plasma methods. *Applied Thermal Engineering* 2015; 90: 120–126.
- [34] Redondoa A B, Bokhovenab J A V. Non-oxidative methane conversion assisted by corona discharge. *Fuel Processing Technology* 2012; 104(6): 265-270.
- [35] Wang W, Snoeckx R, Zhang X, Cha M, Bogaerts A. Modeling Plasma-based CO₂ and CH₄ Conversion in Mixtures with N₂, O₂ and H₂O: the Bigger Plasma Chemistry Picture. *The Journal of Physical Chemistry C* 2018; 122: 8704–8723.
- [36] Chernets N, Kurpad D S, Alexeev V, Rodrigues D B, Freeman T A. Reaction chemistry generated by nanosecond pulsed dielectric barrier discharge treatment is responsible for the tumor eradication in the B16 melanoma mouse model. *Plasma Process and Polymers* 2015; 12(12): 1400–1409.
- [37] Shao T, Wang R, Zhang C, Yan P. Atmospheric-pressure pulsed discharges and plasmas: mechanism, characteristics and applications, *High Voltage* 2018; 3: 14–20.
- [38] Shao T, Long K, Zhang C, Yan P, Zhang S, Pan R. Experimental study on repetitive unipolar nanosecond-pulse dielectric barrier discharge in air at atmospheric pressure. *Journal of Physics D: Applied Physics* 2008; 41(21): 215203.
- [39] Pai D Z, Lacoste D A, Laux C O. Transitions between corona, glow and spark regimes of nanosecond repetitively pulsed discharges in air at atmospheric pressure. *Journal of Physics D: Applied Physics* 2010; 107(9): 093303.
- [40] Xin Y, Sun B, Zhu X, Yan Z, Zhao X, Sun X. Characteristics of hydrogen produced by pulsed discharge in ethanol solution. *Applied Energy* 2016; 168:122–129.
- [41] Xin Y, Sun B, Zhu X, Yan Z, Liu Y, Liu J. Hydrogen production from ethanol decomposition by pulsed discharge with needle-net configurations. *Applied Energy* 2017; 206:126–133.
- [42] Ding M, Hayakawa T, Zeng C, Jin Y, Qi Z, Wang T, Ma L, Yoshiharu Y, Noritatsu T. Direct conversion of liquid natural gas (LNG) to syngas and ethylene using non-equilibrium pulsed discharge. *Applied energy* 2013; 104:777–782.
- [43] Ayan H, Staack D, Fridman G, Gutso A, Mukhin Y, Starikovskii A, Fridman A, Friedman G. Application of nanosecond-pulsed dielectric barrier discharge for biomedical treatment of topographically non-uniform surfaces. *Journal of Physics D: Applied Physics* 2009; 42(12): 125202.
- [44] Jahanmiri A, Rahimpour M R, Shirazi M M, Hooshmanda N, Taghvaei, H. Naphtha cracking through a pulsed DBD plasma reactor: Effect of applied voltage, pulse repetition frequency and electrode material. *Chemical Engineering Journal* 2012; 191: 416-425.

- [45] Jiang N, Hu J, Li J, Shang K, Lu N, Wu Y. Plasma-catalytic degradation of benzene over Ag-Ce bimetallic oxide catalysts using hybrid surface/packed-bed discharge plasmas. *Applied Catalysis B: Environmental* 2016; 184: 355–363.
- [46] Nishida Y, Chiang H C, Chen T C, Cheng C Z. Efficient production of hydrogen by DBD type plasma discharges. *IEEE Transactions on Plasma Science* 2014; 42(12): 3765–3771.
- [47] Khalifeh O, Taghvaei H, Mosallanejad A, Rahimpour M R, Shariati A. Extra pure hydrogen production through methane decomposition using nanosecond pulsed plasma and Pt-Re catalyst. *Chemical Engineering Journal* 2016; 294: 132–145.
- [48] Khalifeh O, Mosallanejad A, Taghvaei H, Rahimpour M R, Shariati A, Yan J. Decomposition of methane to hydrogen using nanosecond pulsed plasma reactor with different active volumes, voltages and frequencies. *Applied Energy* 2016; 169: 585–596.
- [49] Scapinello M, Martini L M, Dilecce G, Tosi, P. Conversion of CH₄/CO₂ by a nanosecond repetitively pulsed discharge. *Journal of Physics D: Applied Physics* 2016; 49(7): 075602.
- [50] Rouso A, Yang S, Lefkowitz J, Sun W, Ju Y. Low temperature oxidation and pyrolysis of n-heptane in nanosecond-pulsed plasma discharges. *Proceedings of the Combustion Institute* 2016; 36(3): 4105–4112.
- [51] Shao T, Zhang C, Long K, Zhang D, Wang J, Yan P, Zhou Y. Surface modification of polyimide films using unipolar nanosecond-pulse DBD in atmospheric air. *Applied Surface Science* 2010; 256(12): 3888–3894.
- [52] Shao T, Zhang C, Yu Y, Fang Z, Yan P. Temporal evolution of nanosecond-pulse dielectric barrier discharges in open air. *EPL* 2012; 97(5): 55005.
- [53] Zhang C, Shao T, Zhou Y, Fang Z, Yan P. Effect of O₂ additive on spatial uniformity of atmospheric-pressure helium plasma jet array driven by microsecond-duration pulses. *Applied Physics Letters* 2014; 105(4): 044102.
- [54] Shao T, Yang W, Zhang C, Niu Z. Enhanced surface flashover strength in vacuum of polymethylmethacrylate by surface modification using atmospheric-pressure dielectric barrier discharge. *Applied Physics Letters* 2014; 105(7): 071607.
- [55] Peng J, Chen N, He R, Wang Z, Dai S, Jin X. Electrochemically Driven Transformation of Amorphous Carbons to Crystalline Graphite Nanoflakes: A Facile and Mild Graphitization Method. *Angewandte Chemie* 2017; 129(7): 1777–1781.
- [56] Tu X, Whitehead J C. Plasma dry reforming of methane in an atmospheric pressure AC gliding arc discharge: Co-generation of syngas and carbon nano materials. *International Journal of Hydrogen Energy* 2014; 39(18):9658–9669.
- [57] Hooshmand N, Rahimpour MR, Jahanmiri A, Taghvaei H, Shirazi M. Hexadecane cracking in a hybrid catalytic pulsed dielectric barrier discharge plasma reactor. *Industrial & Engineering Chemistry Research* 2013; 52(12): 4443–4449.
- [58] Song H K, Lee H, Choi J W, Na B K. Effect of electrical pulse forms on the CO₂, reforming of methane using atmospheric dielectric barrier discharge. *Plasma Chemistry & Plasma Processing* 2004; 24(1): 57–72.
- [59] Tu X, Whitehead J C. Plasma-catalytic dry reforming of methane in an atmospheric dielectric barrier discharge: Understanding the synergistic effect at low temperature. *Applied Catalysis B Environmental* 2012; 125(33):439–448.
- [60] Heintze M, Magureanu M. Methane conversion into acetylene in a microwave plasma:

- Optimization of the operating parameters. *Journal of Applied Physics*, 2002; 92(5): 2276–2283.
- [61] Xu C, Tu X. Plasma-assisted methane conversion in an atmospheric pressure dielectric barrier discharge reactor. *Journal of Energy Chemistry*, 2013; 22(3): 420–425.
- [62] Liao M, Wang Y, Wu H, Li H, Xia W. Study of non-thermal DC arc plasma of CH₄/Ar at atmospheric pressure using optical emission spectroscopy and mass spectrometry. *Plasma Science and Technology* 2015; 17(9): 743–748.
- [63] De Bie C, Verheyde B, Martens T, Van Dijk J, Paulussen S, Bogaerts A. Fluid modeling of the conversion of methane into higher hydrocarbons in an atmospheric pressure dielectric barrier discharge. *Plasma Processes and Polymers* 2011; 8(11): 1033–1058.
- [64] Hagelaar G J M, Pitchford L C. Solving the Boltzmann equation to obtain electron transport coefficients and rate coefficients for fluid models *Plasma Sources Science & Technology* 2005; 14(4):722.
- [65] Wang Y, Li C, Shi J, Wu X, Ding H. Measurement of electron density and electron temperature of a cascaded arc plasma using laser Thomson scattering compared to an optical emission spectroscopic approach. *Plasma Science and Technology* 2017, 19(11): 115403.
- [66] Kinema Research and Software, LXcat. <https://nl.lxcat.net/cache/5b0124d67975f/>; 2017 [accessed 15 July 2017].
- [67] Rueangjitt N, Sreethawong T, Chavadej S, Sekiguchi H L. Plasma-catalytic reforming of methane in AC microsized gliding arc discharge: Effects of input power, reactor thickness, and catalyst existence. *Chemical Engineering Journal* 2009; 155(3): 874–880.
- [68] Morgan W L. A critical evaluation of low-energy electron impact cross sections for plasma processing modeling. II: Cl₄, SiH₄, and CH₄. *Plasma Chemistry Plasma Processing* 1992; 12(4): 477–493.
- [69] Gangoli S P. Experimental and modeling study of warm plasmas and their applications. Ann Arbor, ProQuest, 2007.
- [70] Wang W, Patil B, Heijkers S, Hessel V, Bogaerts A. Nitrogen fixation by gliding arc plasma: better insight by chemical kinetics modelling. *ChemSusChem* 2017; 10: 2145–2157.
- [71] Scapinello M, Delikonstantis E, Stefanidis G D. The panorama of plasma-assisted non-oxidative methane reforming. *Chemical Engineering and Processing: Process Intensification* 2017; 17:120–140
- [72] Chen H L, Lee H M, Chen S H, Chao Y, Chang M B. Review of plasma catalysis on hydrocarbon reforming for hydrogen production—Interaction, integration, and prospects. *Applied Catalysis B Environmental* 2008; 85(1-2):1–9.
- [73] Horvath G, Mason N J, Polachova L, Zhoran M, Moravsky L, Matejcik S. Packed bed DBD discharge experiments in admixtures of N₂ and CH₄. *Plasma Chemistry & Plasma Processing* 2010; 30(5):565–577.
- [74] Nozaki T, Hattori A, Okazaki K. Partial oxidation of methane using a microscale non-equilibrium plasma reactor. *Catalysis Today* 2004; 98(4):607–616.
- [75] Ravasio S, Cavallotti C. Analysis of reactivity and energy efficiency of methane conversion through non thermal plasmas. *Chemical Engineering Science* 2012; 84(52):580–590.
- [76] Dors M, Nowakowska H, Jasiński M, Mizeraczyk J. Chemical kinetics of methane pyrolysis in microwave plasma at atmospheric pressure. *Plasma Chemistry & Plasma Processing* 2014;

34(2):313–326.

[77] Fridman A. Plasma chemistry. Cambridge (UK): Cambridge University Press; 2008, p. 589-601.

List of figure captions

Fig. 1. Schematic of the experimental apparatus and diagnostic system.

Fig. 2. Typical voltage-current waveforms of pulsed spark discharges: (a) nanosecond pulsed spark discharge, (b) microsecond pulsed spark discharge. (Gas flow rate: 50 mL/min, frequency: 1 kHz, gap length: 6 mm).

Fig. 3. The effect of gap length on CH₄ conversion and gas products distribution in the nanosecond pulsed spark discharge: (a) CH₄ conversion and gas product yields, (b) selectivity of gas products, (c) carbon and hydrogen balances. (Gas flow rate: 50 mL/min, frequency: 1 kHz).

Fig. 4. The effect of gap length on CH₄ conversion and gas products distribution in the microsecond pulsed spark discharge: (a) CH₄ conversion and gas product yields, (b) selectivity of gas products, (c) carbon and hydrogen balances. (Gas flow rate: 50 mL/min, frequency: 1 kHz).

Fig. 5. The effect of gas flow rate on CH₄ conversion and gas products distribution in the nanosecond pulsed spark discharge: (a) CH₄ conversion and gas product yields, (b) selectivity of gas products, (c) carbon and hydrogen balances. (Frequency: 1 kHz, gap length: 6 mm).

Fig. 6. The effect of gas flow rate on CH₄ conversion and gas products distribution in the microsecond pulsed spark discharge: (a) CH₄ conversion and gas product yields, (b) selectivity of gas products, (c) carbon and hydrogen balances. (Frequency: 1 kHz, gap length: 6 mm).

Fig. 7. The SEM images and Raman spectra of nano-carbon particles: (a) area 1, (b) area 2.

Fig. 8. CH₄ conversion and *ECE* as a function of *SEI*: (a) CH₄ conversion, (b) *ECE*. (Blue/red scatter represents micro-/nano- second pulsed spark discharge).

Fig. 9. Typical optical emission spectra of pulsed spark discharges: (a) nanosecond pulsed spark discharge, (b) microsecond pulsed spark discharge. (Gas flow rate: 50 mL/min, frequency: 1 kHz, gap length: 6 mm).

Fig. 10. Schematic diagram of CH₄ cracking process in pulsed needle–plate discharge plasma. (The width of arrows indicates the possibility fraction of each channels).

Table 1. Characteristics and parameters of plasma produced by different pulsed power sources at different gap lengths.

Power source	D (mm)	P (W)	<i>Mean</i> E/N (Td)	<i>Mean</i> N_e (cm ⁻³)	<i>Mean</i> T_e (eV)	<i>Mean</i> T_v (K)
Nanosecond pulse power	4	12.7	20.4	1.1E+16	2.0	6800
	6	14.8	16.5	9.3E+15	1.7	6670
	8	16.3	11.6	5.3E+15	1.3	6450
	10	20.0	9.4	7.24E+15	1.1	5400
Microsecond pulse power	2	10.1	31.5	1.41E+14	2.6	9450
	4	19.6	18.2	2.79E+14	1.9	7350
	6	24.3	14.5	4.6E+14	1.6	6150